



**HAL**  
open science

## Small Structural Differences between Two Ferrocenyl Diphenols Determine Large Discrepancies of Reactivity and Biological Effects

Federica Tonolo, Michèle Salmain, Valeria Scalcon, Siden Top, Pascal Pigeon, Alessandra Folda, Benoît Caron, Michael James Mcglinchey, Robert-Alain Toillon, Alberto Bindoli, et al.

► **To cite this version:**

Federica Tonolo, Michèle Salmain, Valeria Scalcon, Siden Top, Pascal Pigeon, et al.. Small Structural Differences between Two Ferrocenyl Diphenols Determine Large Discrepancies of Reactivity and Biological Effects. *ChemMedChem*, 2019, 14 (19), pp.1717-1726. 10.1002/cmdc.201900430 . hal-02282225

**HAL Id: hal-02282225**

**<https://hal.sorbonne-universite.fr/hal-02282225>**

Submitted on 24 Oct 2019

**HAL** is a multi-disciplinary open access archive for the deposit and dissemination of scientific research documents, whether they are published or not. The documents may come from teaching and research institutions in France or abroad, or from public or private research centers.

L'archive ouverte pluridisciplinaire **HAL**, est destinée au dépôt et à la diffusion de documents scientifiques de niveau recherche, publiés ou non, émanant des établissements d'enseignement et de recherche français ou étrangers, des laboratoires publics ou privés.

## SMALL STRUCTURAL DIFFERENCES BETWEEN TWO FERROCENYL DIPHENOLS DETERMINE LARGE DISCREPANCIES OF REACTIVITY AND BIOLOGICAL EFFECTS

Federica Tonolo,<sup>a</sup> Michèle Salmain,<sup>b</sup> Valeria Scalcon,<sup>a</sup> Siden Top,<sup>b</sup> Pascal Pigeon,<sup>b,c</sup> Alessandra Folda,<sup>a</sup> Benoit Caron,<sup>d</sup> Michael J. McGlinchey,<sup>e</sup> Alberto Bindoli,<sup>f</sup> Gérard Jaouen,<sup>b,c</sup> Anne Vessières,<sup>\*b</sup> Maria-Pia Rigobello<sup>\*a</sup>

a) Dipartimento di Scienze Biomediche, Università di Padova, Via Ugo Bassi 58/b, 35131 Padova, Italy.

b) Sorbonne Université, CNRS, IPCM, 4 Place Jussieu, 75005 Paris, France.

c) Chimie ParisTech, PSL University, 11 rue Pierre et Marie Curie, 75005 Paris, France

d) Sorbonne Université, IStEP, ALIPP6, 4 Place Jussieu, 75005 Paris, France

e) School of Chemistry, University College Dublin, Belfield, Dublin 4, Ireland

f) Istituto di Neuroscienze (CNR) Sezione di Padova, c/o Dipartimento di Scienze Biomediche, Via Ugo Bassi 58/b, 35131 Padova, Italy.

\* To whom correspondence should be sent

A. Vessières: [anne.vessieres@sorbonne-universite.fr](mailto:anne.vessieres@sorbonne-universite.fr)

M.P. Rigobello: [mariapia.rigobello@unipd.it](mailto:mariapia.rigobello@unipd.it)

**Abstract:** The ferrocenyl diphenol complexes 1,1-bis(4'-hydroxyphenyl)-2-ferrocenyl-but-1-ene (**1**) and 1,2-bis(4'-hydroxyphenyl)-1-ferrocenyl-but-1-ene [(*Z*)-**2**], which differ by the relative position of the two phenolic substituents, display dramatically different antiproliferative activities on cancer cells (**1** is far more cytotoxic than **2**). In this study, our goal was to discover the origin of this difference by comparing their reactivity and biological behaviour. In terms of common behaviour, we found that **1** and **2** are both efficient inhibitors of thioredoxin reductase (TrxR) in vitro after oxidation by a horseradish peroxidase/H<sub>2</sub>O<sub>2</sub> system. However, as **1** is only a moderate inhibitor of TrxR in MDA-MB-231 cells, TrxR is probably not the major target responsible for the cytotoxicity of **1**. In terms of differences, we noted that **1** induced a significant redox imbalance characterised by lipid peroxidation and thiol oxidation, and a

moderate decrease of the mitochondrial membrane potential in breast cancer cells, whereas **2** has almost no effect. These results underline the importance of the *trans* configuration in the ferrocenyl–double bond–phenol motif, which is present in **1** but is *cis* in (*Z*)-**2**.

## Introduction

Metalloodrugs based on the coordination chemistry of platinum, such as cisplatin, carboplatin and oxaliplatin, are used alone or in combination in over 50 % of cancer treatments.<sup>1-3</sup> It is nevertheless well recognised that despite their proven capabilities, these drugs have serious issues, including a general toxicity linked to their lack of selectivity between healthy and damaged cells, a fairly narrow therapeutic range and a tendency to give rise to resistance.<sup>1</sup> This has led to research into other metalloodrugs bearing different metals as well as different types of bonding such as those described by organometallic chemistry and characterised by covalent metal–carbon (M–C) bonds.<sup>2, 4, 5</sup> The development of bioorganometallic chemistry with its novel functionalities has provided access to innovative properties that make it possible to address different biological targets.<sup>4-7</sup> In this context, we have developed species incorporating ferrocene onto the tamoxifen skeleton, thus providing a new angle from which to evaluate what can be achieved with antitumour agents (protein targets, selectivity for cancerous cells, avoidance of resistance effects, multiple mechanisms).<sup>8-12</sup> This family of complexes, known as ferrocifens, share a “ferrocenyl–alkene–phenol” redox motif, which generates organometallic quinone methides (QMs) as primary metabolites, the electrophilicity of which can be modulated by changing their substituents.<sup>8, 13-16</sup> Ferrocifens are proving, both chemically and biologically, to be a very rich resource.<sup>9-12, 17</sup>

In the ferrocifen family, the diphenolic complex **1** (Figure 1) was one of the first to be synthesised and studied. It was initially designed for investigating the influence of the dimethylaminopropyl substituent in **3** on its cytotoxic activity toward the hormone-independent breast cancer cell line MDA-MB-231.<sup>18, 19</sup> Fortuitously, the cytotoxic activities of **1** and **3** were similar ( $IC_{50}$ =0.6 and 0.5  $\mu$ M, respectively, on MDA-MB-231 cells), which makes them hits among this family of compounds, which also includes the ansa-ferrociphenol complex **5**.<sup>10, 20</sup> Complex **1**, formulated in lipid nanocapsules, was also the first in the family to show an antitumour effect *in vivo* on

rats with ectopic or orthotopic implanted tumours from glioblastoma (rat 9 L cells).<sup>10, 11, 21</sup> However, limited cell biology studies on **1** were performed on glioma and melanoma cell lines.<sup>22, 23</sup>

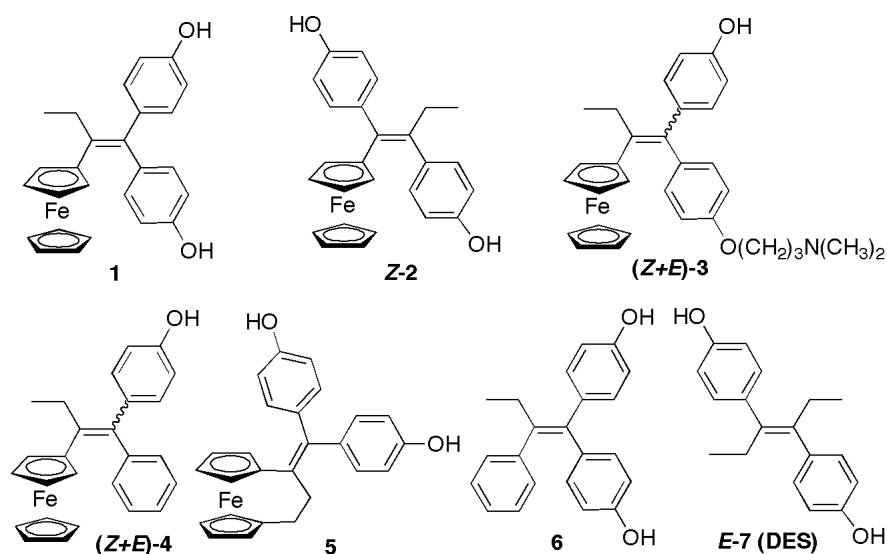


**Figure 1.** Structures of ferrocenyl complexes discussed in this paper and their corresponding organic molecules.

Subsequently, the ferrocenyl diphenol **2**, a regioisomer of **1** differing in the position of the two phenolic substituents on the central carbon-carbon double bond, was synthesised but its cytotoxicity was unexpectedly much lower than that of **1**.<sup>24, 25</sup> Recent results on **4**, the monophenol ferrocenyl complex, suggested that the mechanism of action of phenolic ferrocifens might differ from that of the tamoxifen-like complex **3**.<sup>26</sup> This difference was associated with the presence on **3** of the dimethylaminopropyl side chain. Recently, the QM of **3** was found to have strong inhibitory activity on the enzyme thioredoxin reductase (TrxR).<sup>26</sup> TrxR belongs to the thioredoxin system, which, together with the glutathione system, is responsible for thiol redox balance. TrxR displays a selenocysteine residue at its C-terminal active site, which acts as a major target of electrophiles as well as many metal complexes.<sup>26-30</sup> TrxR is often overexpressed in many cancer cell lines and its inhibition brings about cell death.<sup>26, 28-30</sup> Here, we report the results of a set of experiments on **1** and **2** carried out in an attempt to rationalise their difference in cytotoxicity and also to give clues concerning their possible mechanism of action. For

this purpose, two breast cancer cell lines—one hormone dependent (MCF-7), the other triple-negative, hormone independent (MDA-MB-231)—were used.

## Results

The syntheses of **1** and **2** were accomplished using the McMurry cross-coupling reaction of ketones according to a published procedure.<sup>19, 24, 25</sup> Interestingly, complex **2** is obtained mainly as the *Z* isomer (*Z/E*, 93:7) whereby the two phenol groups are *trans* disposed. In addition, it was found that (*Z*)-**2** does not isomerise significantly even after one week in DMSO (*Z/E*, 99:1).<sup>24</sup> Complex **2** is the organometallic analogue of (*E*)-**7** (diethylstilbestrol, DES), and also undergoes slow isomerisation.<sup>31</sup> The almost exclusive formation of (*Z*)-**2**, and its resistance to isomerisation, is attributed to the steric problems that arise by positioning the two phenol moieties face to face in (*E*)-**2**. Preferential formation of (*Z*)-**2** in the McMurry reaction is determined by the transition state for radical coupling in which steric factors are minimised.<sup>32</sup>

## Enzymatic oxidation studies of **1**, **2** and the organic molecules **6** and **7** with the horseradish peroxidase (HRP)/H<sub>2</sub>O<sub>2</sub> system

Enzymatic oxidation reactions were performed with a fourfold molar excess of H<sub>2</sub>O<sub>2</sub> in the presence of HRP at pH 8.1 or 5.0 and were monitored by UV/Vis spectroscopy.

### Enzymatic oxidation of **1** and **6**

For **1**, a bright pink adduct ( $\lambda_{\text{max}}=565$  nm) was formed rapidly at pH 8.1 (Figure 2, upper panel), whereas the same experiment performed at pH 5 afforded a yellow adduct ( $\lambda_{\text{max}}=416$  nm; Figure S1 in the Supporting Information, upper panel). If the experiment was performed at pH 6.8, we observed the presence of the two bands (Figure S1, lower panel). This behaviour is reminiscent of that previously observed for the ansa-ferrociphenol derivative **5**,<sup>33</sup> which lets us conclude that enzymatic oxidation of **1** affords the corresponding QM in the anionic phenolate form **8 A** at pH

8.1, the neutral phenolic form **8 B** at pH 5.0 (Scheme 1), or as a mixture of **8 A** and **8 B** at the intermediate pH 6.8.

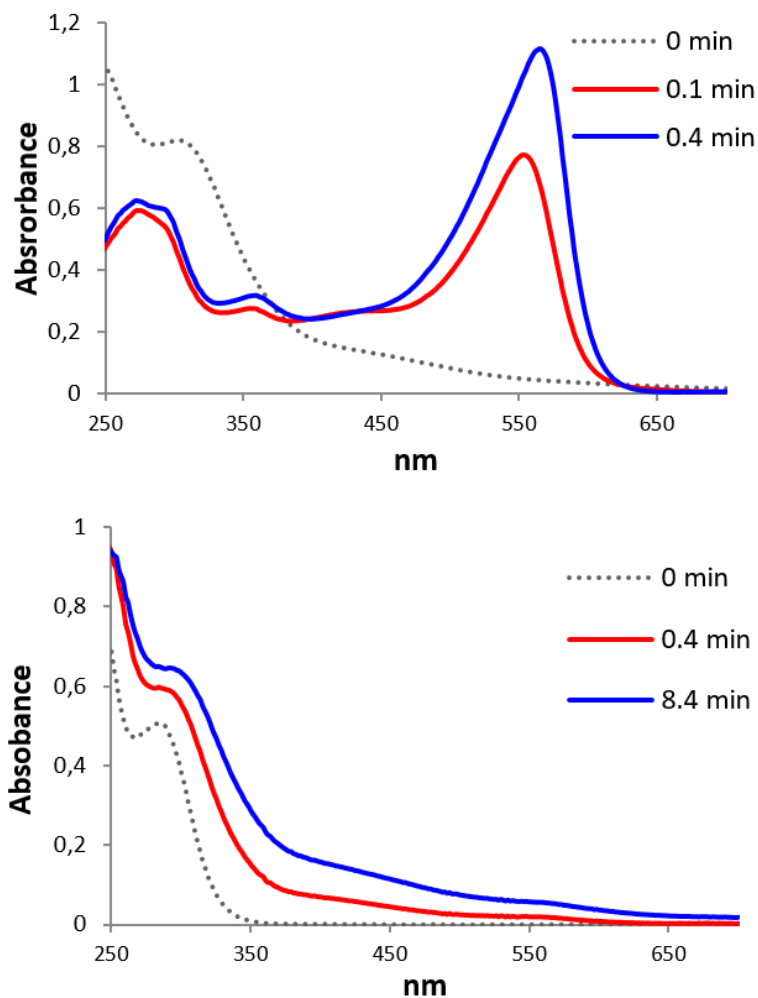
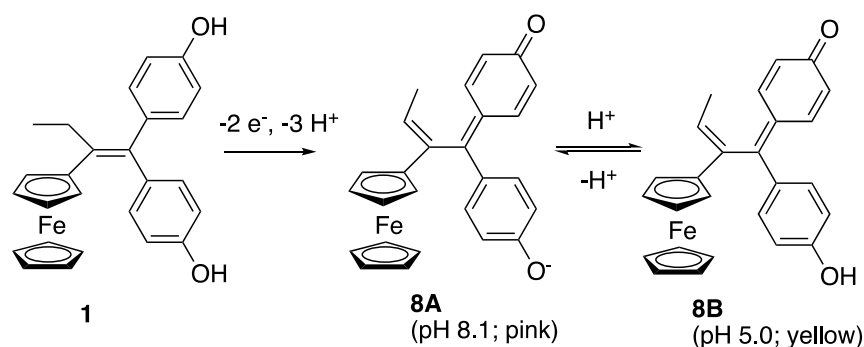


**Figure 2.** Time evolution of the UV/Vis spectrum of 50  $\mu\text{M}$  **1** (upper panel) and **6** (lower panel) at 25 °C in the presence of HRP (46 nM) and  $\text{H}_2\text{O}_2$  (200  $\mu\text{M}$ ) at pH 8.1 (0.2 M Tris-HCl, 1 mM EDTA, 10 % DMSO). Upper panel: pure **1** (0 min), band centred at 304 nm; after 0.1 min: bands at 553 (very intense), 358 (weak) and 279 nm (broad, medium); after 0.4 min: bands at 565 (intense), 358 (weak) and 279 nm (broad, medium). Lower panel: pure **6** (0 min) band centred at 284 nm; after 0.4 and 8.4 min: shoulder at 296 nm.



**Scheme 1.** Proposed sequence of the enzymatic oxidation of **1** by an HRP/H<sub>2</sub>O<sub>2</sub> mixture.

The rate of formation of the QM of **1** at pH 8.1 was much faster than that of **5** [rate constant  $k=2.5 \text{ min}^{-1}$  for **1** (Figure S2) vs.  $0.12 \text{ min}^{-1}$  for **5** at pH 8];<sup>33</sup> its half-life is 12 min, and no intermediate was observed by UV/Vis spectroscopy. These differences can be explained in terms of the ring strain inherent in the ansa structure of **5**. Complex **8B** had been prepared previously by chemical oxidation with Ag<sub>2</sub>O and characterised by NMR spectroscopy,<sup>34</sup> but could not be obtained in the solid state due to its lower stability compared to that of the QM of **4**, which could be isolated.<sup>26</sup>

Complex **1** is the organometallic analogue of **6**, and interestingly, its treatment, in the same conditions, afforded non-identified compounds at both pH 8.1 (Figure 2, lower panel) and pH 5.0 (Figure S3), but certainly not the QM. This indicates that the presence of the redox-active ferrocenyl unit on complex **1** was essential to drive QM formation under oxidative conditions.

## Enzymatic oxidation of **2** and **7**

Enzymatic oxidation of **2** at pH 8.1 led to the immediate formation of a blue-green adduct ( $\lambda_{\text{max}}=302, 408$  and  $675 \text{ nm}$ ) followed by its conversion into another greenish product ( $\lambda_{\text{max}}=393$  and  $629 \text{ nm}$ ; Figure 3, upper panel).

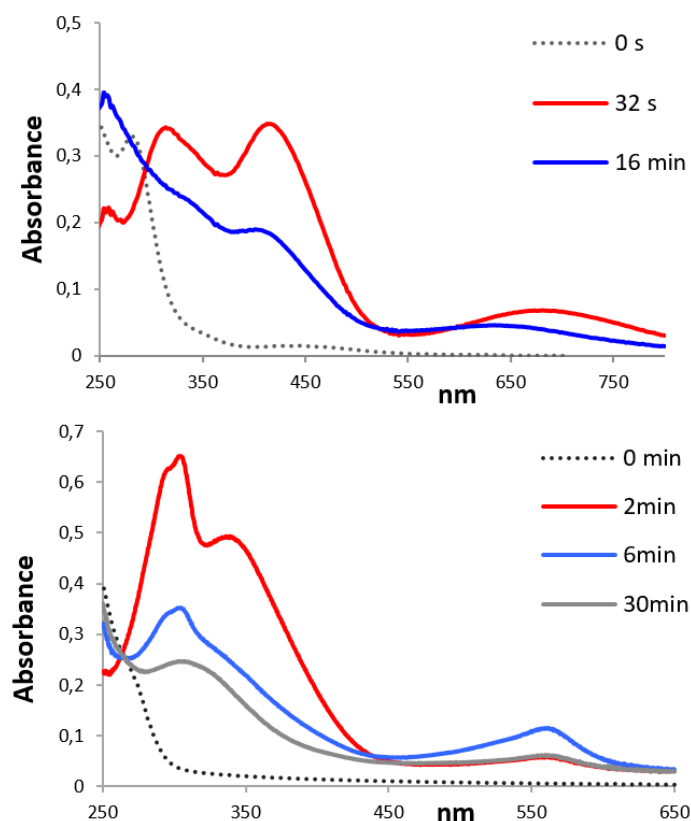
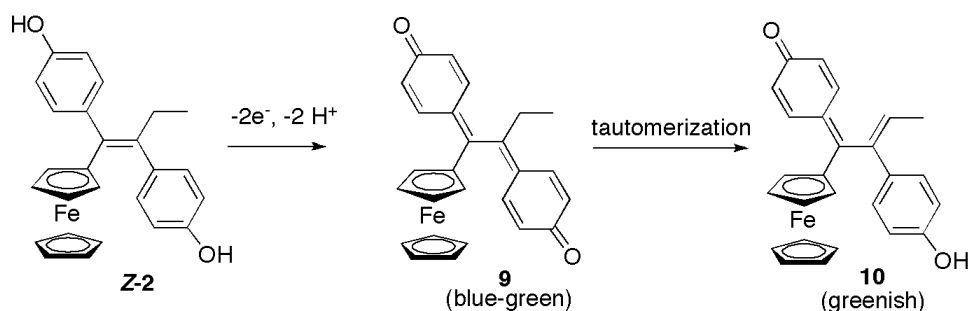


**Figure 3.** Time evolution of the UV/Vis spectrum of 50  $\mu\text{M}$  **2** (upper panel) and **7** (lower panel) at 25  $^{\circ}\text{C}$  in the presence of HRP (46 nM) and  $\text{H}_2\text{O}_2$  (200  $\mu\text{M}$ ) at pH 8.1 (0.2 M Tris-HCl, 1 mM EDTA, 10 % DMSO). Upper panel: pure **2** (0 min): band centred at 284 nm; after 32 s: bands at 683 (broad and weak), 416 and 316 nm (intense); after 16 min: bands at 638 (broad and weak) and 408 nm (intense). Lower panel: pure **7** (0 min) no characteristic bands; after 2 min: bands centred at 304 and 338 nm (intense); after 6 min: bands at 306 (intense) and 561 nm (broad and weak), after 30 min these two bands dramatically decreased in intensity.

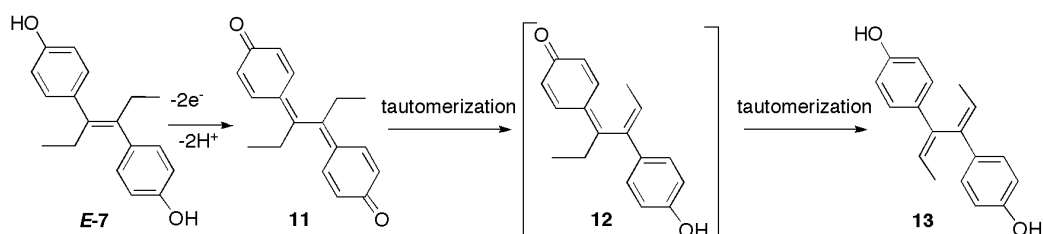
The colour of the first species is reminiscent of that of a ferrocenium species, which, according to the previously established mechanism of oxidation of ferrocifens, is the first intermediate to be formed in the sequence of reactions leading to a QM (Scheme S1).<sup>17</sup> However, an electron paramagnetic resonance (EPR) experiment using a mixture of **2** and  $\text{H}_2\text{O}_2$ /HRP after a short incubation time invalidated this hypothesis, because no signal corresponding to an iron-centred radical was detected. Indeed, chemical oxidation of **2** by  $\text{Ag}_2\text{O}$  was previously found to afford the phenol quinone compound **10** resulting from the loss of two electrons and two protons (Scheme 2).<sup>24</sup> This species was characterised by various spectroscopic techniques; the UV/Vis spectrum showed two characteristic bands centred at 392 and 590 nm in acetonitrile.



**Scheme 2.** Sequence of the oxidation of **2** involving loss of 2 electrons and 2 protons leading to **9**, the diquinone methide, then by tautomerisation to the phenol-QM **10**.<sup>24</sup>

The mechanism of the oxidation of **2** to **10** is a two-step process in which the diphenol compound is first rapidly converted into the diquinone **9**, which undergoes subsequent tautomerisation to afford **10**, the phenol–quinone.

For comparison, the well-known estrogenic molecule **7** was enzymatically oxidised in the same way, and the UV/Vis spectrum of the mixture was recorded over a period of 30 min (Figure 3, lower panel). Bands centred at 304 and 338 nm appeared within 2 min, and were readily assigned to the diquinone derivative **11** (Scheme 3). The system gradually evolved toward another species absorbing at 306 and 560 nm. It has been reported that **11** undergoes successive tautomerisations from **12** to **13** by migration of protons from the two ethyl substituents to afford the diphenol (Scheme 3).<sup>35</sup> The rate of conversion between **12** and **13** increased with the pH.<sup>35</sup> Compound **12**, the product of monotautomerisation of **11**, the phenol–quinone analogous to **10**, the final oxidation product of complex **2**, has never been isolated. This second tautomerisation is possible for **12** but not for **10**.



**Scheme 3.** Sequence of the oxidation of (*E*-**7**) involving loss of 2 electrons and 2 protons leading to **11**, the diquinone methide, then by a double tautomerisation to the diphenol **13**.<sup>35</sup>

## Study of inhibition of cytosolic TrxR by 1 and 2

To compare **1** and **2** with other ferrocenyl complexes, the potential effects on TrxR were investigated. Therefore, their inhibition of the isolated and purified cytosolic isoform of thioredoxin reductase (TrxR1) was measured. In accordance with previous results,<sup>28, 36</sup> we tested the action of **1** and **2** alone, and the compounds obtained by enzymatic oxidation by the HRP/H<sub>2</sub>O<sub>2</sub> mixture of **1** and **2**, that is, **8 A** and **10**, respectively. Compounds **1** and **2** only moderately inhibited cytosolic TrxR1 (IC<sub>50</sub>=19.36 μM and 32.2 μM, respectively), whereas **8 A** and **10** were strong TrxR1 inhibitors (IC<sub>50</sub>=27 nM and 31 nM, respectively; Figure 4). These values were lower than that found previously for **3** (IC<sub>50</sub>=60 nM).<sup>28</sup> No inhibition of glutathione reductase (GR) by **1**, **2**, **8 A** and **10** was detected under similar conditions (Figure S4).

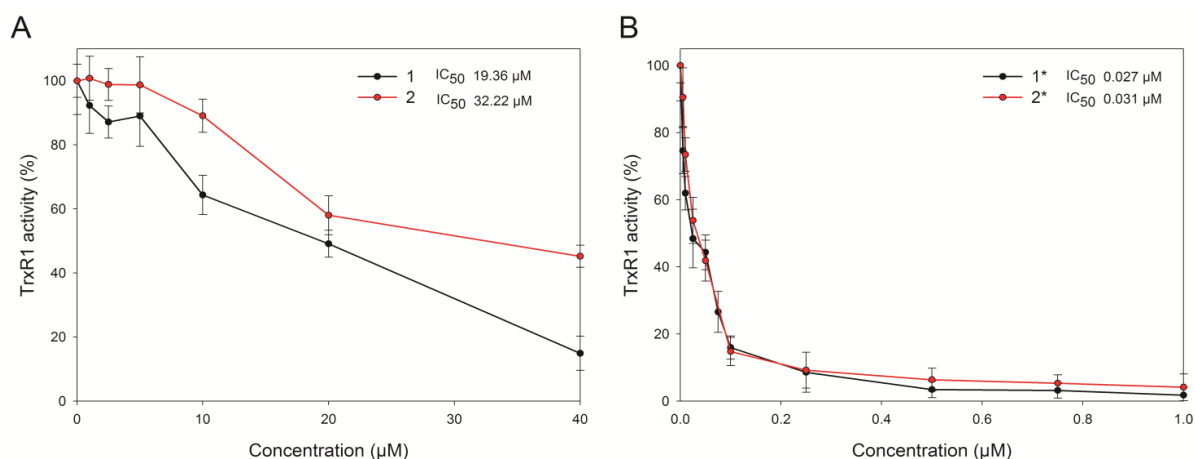


**Figure 4.** Concentration-dependent effects of A) **1** and **2**, and B) **8 A** and **10** (obtained after oxidation of **1** and **2** by the HRP/H<sub>2</sub>O<sub>2</sub> mixture for 15 min), on the cytosolic thioredoxin reductase activity (see the Experimental Section for details).

## Mechanism of inhibition of TrxR1 by 1 and 2

The biotin-conjugated iodoacetamide (BIAM) assay was used in order to gain information on the residues involved in the inhibition of TrxR1 induced by **1**, **2**, **8 A** and **10**. This assay evaluates the ability of the complexes to interact with the thiol and/or selenol groups borne by the cysteine and selenocysteine residues of the enzyme. BIAM alkylates thiol and selenol groups depending on the pH. At pH 6.0,

only selenocysteine and low pKa cysteine residues were alkylated, whereas at pH 8.5, both selenocysteine and accessible cysteine residues were derivatised by BIAM. As shown in Figure 5, and in agreement with the TrxR1 inhibition pattern reported in Figure 4, both **8 A** and **10** prevented the alkylation of TrxR1 by BIAM at pH 6 (**8 A** being slightly more efficient than **10**), indicating that both compounds were able to interact with the selenol group. At pH 8.5, full inhibition of BIAM alkylation by **8 A** and **10** occurred, indicating that they were also able to interact with accessible cysteine residues. In contrast, compounds **1** and **2** alone were barely effective. This type of result has been found previously for the ansa-ferrociphenol derivative **5**,<sup>33</sup> whereas only derivatisation of selenocysteine was observed with **3**.<sup>26</sup>

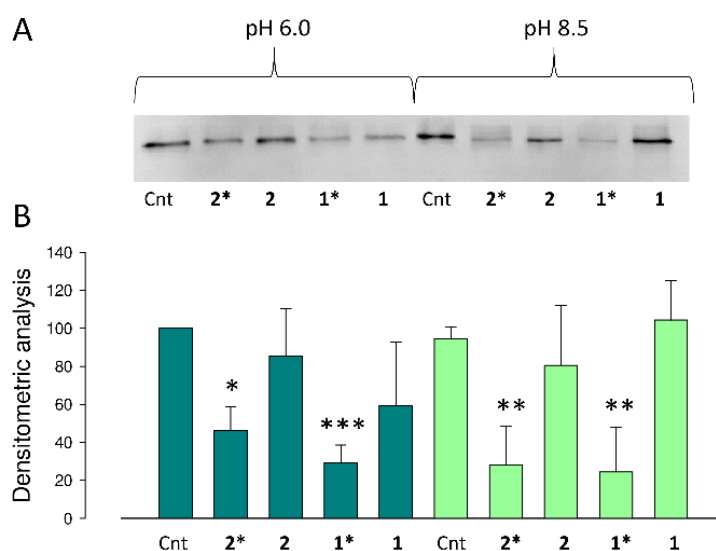


**Figure 5.** A) Biotinylated iodoacetamide (BIAM) assay of TrxR1 treated with **1**, **8 A**, **2** or **10**. The complexes and their derivatives were incubated in the presence of a pre-reduced aliquot of TrxR1, as reported in the Experimental Section. Then, aliquots of the reaction mixture were added to 50 mM BIAM in buffer at either pH 6.0 (0.1 m HEPES–Tris) or pH 8.5 (0.1 m Tris·HCl) to alkylate the remaining SH/SeH groups. B) Densitometric analysis was performed using ImageJ software. \* $p < 0.05$ ; \*\* $p < 0.01$ ; \*\*\* $p < 0.001$ .

## Antiproliferative activity of **1** and **2** on breast cancer cells

The antiproliferative activity of **1** and **2** was measured in two breast cancer cell lines (MDA-MB-231 and MCF-7) after 72 h by MTT cell viability assay. Complex **1**

exhibited high antiproliferative activity on both cancer cells lines ( $IC_{50}$ =0.98 and 0.7  $\mu$ M, respectively), whereas complex **2** was markedly less cytotoxic ( $IC_{50}$ =69.8 and 25.5  $\mu$ M, respectively). This result confirmed the low cytotoxicity previously described for **2**.<sup>24, 25</sup>

### **Inhibition of TrxR and GR induced by 1 and 2 in breast cancer cells**

Next, we evaluated the inhibitory effects of **1** and **2** on TrxR and GR activity in breast cancer cells. The enzymatic activity was measured in cell lysates, after incubation of cells with **1** or **2** at 20 or 40  $\mu$ M for 18 h (Figure 6). Complex **1** induced a moderate inhibition of TrxR (around 25 %) in MDA-MB-231 cells, but no inhibition in MCF-7 cells, whereas **2** had almost no effect on either cell line (Figure 6 A). Compounds **1** and **2** had almost no effect on GR activity, at either concentration, in the two cell lines (Figure 6 B). We also found that, under similar conditions (15  $\mu$ M, 18 h), **1** had no inhibitory effect on TrxR activity in Jurkat cells (Figure S5). Such different behaviour toward TrxR in cancer cells and in vitro on purified enzyme has been previously observed for the monophenol complex **4**.<sup>26</sup> Those observations were rationalised by the further conversion of its QM into an indene in protic solvent. Indeed, indene **14** is readily obtained by treating **1** with  $Ag_2O$  as oxidant, followed by  $ZnCl_2$  as Lewis acid (Scheme 4). In addition, it was also identified as one of the metabolites during the microsomal oxidation of **1**.<sup>37</sup> In contrast to the QM, the indene cannot undergo Michael additions, which might explain the limited inhibition of TrxR by **1** in cancer cells. This result suggests that inhibition of TrxR does not play a major role in the cytotoxicity of **1**.

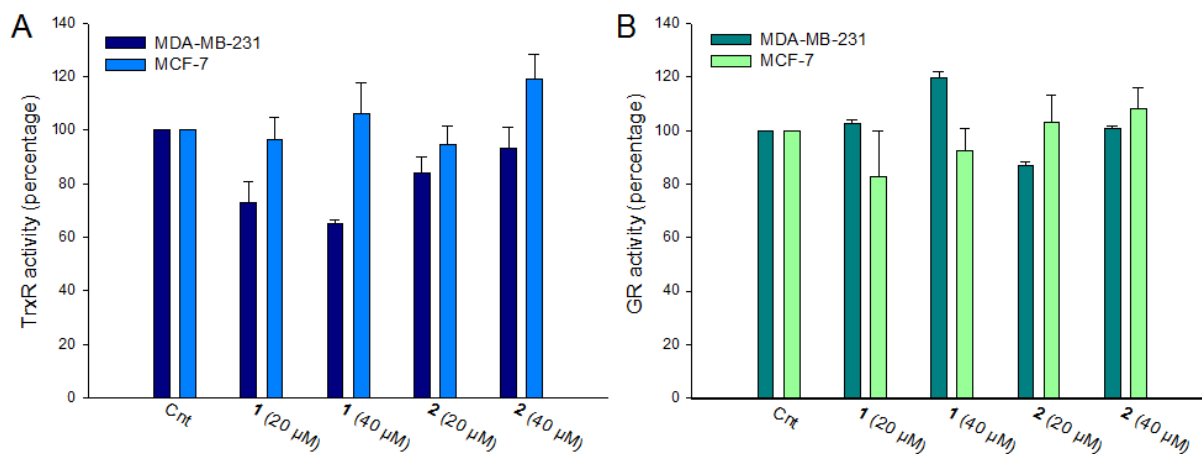
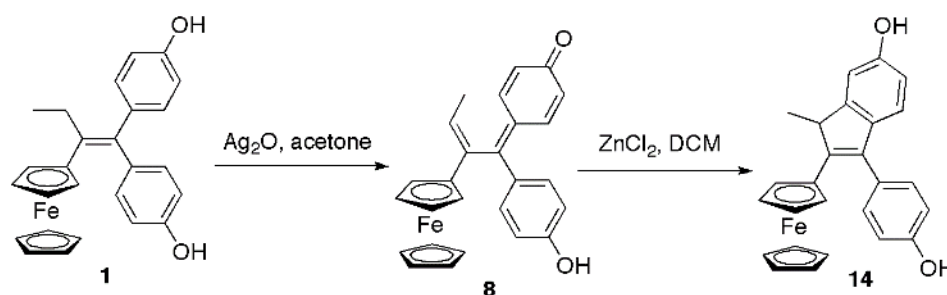


**Figure 6.** Effect of **1** and **2** on A) TrxR and B) GR enzyme activities in MDA-MB-231 and MCF-7 cells.



**Scheme 4.** Formation of the indene **14** from compound **1**.<sup>37</sup>

## Quantification of total thiols in cancer cells incubated with **1** or **2**

Intracellular sulfhydryl groups exist as thiol/thiolates or disulfide forms depending on the redox state of cells. In addition to protein thiols, the most abundant low-molecular-weight thiol in cells is glutathione, present at millimolar concentration. To investigate the action of **1** and **2** on the cellular redox balance, the total thiol content in cells treated with 40  $\mu$ M of **1** or **2** for 18 h was quantified (Table 1). The results showed that **1** induced a strong redox imbalance in MDA-MB-231 cells (44 % decrease of thiol content) and a less pronounced action in MCF-7 cells (18 % decrease of thiols), whereas **2** has almost no effect.

**Table 1.** Quantification of total thiols in control cells and cells incubated with **1** or **2** (40  $\mu$ M, 18 h).

Total thiols (nmol per mg protein)		
Compound	MDA-MB-231	MCF-7
None	38.2 $\pm$ 7.8	48.9 $\pm$ 7.9

<b>1</b>	21.3 ± 0.6	40.2 ± 5.1
<b>2</b>	40.6 ± 5.1	46.1 ± 7.8

### Evaluation of the mitochondrial membrane potential in cancer cells treated with 1 or 2

The mitochondrial membrane potentials (MMPs) in MDA-MB-231 and MCF-7 cells were evaluated by flow cytometry using the fluorescent dye tetramethylrhodamine methyl ester (TMRM). Complex 1 induced a significant decrease of MMP in both MDA-MB-231 and MCF-7 cells (30 % of cells with low MMP after 18 h in the presence of 1 at 40 µM), whereas complex 2 was scarcely effective (Figure 7); 1 had no effect on Jurkat cells.

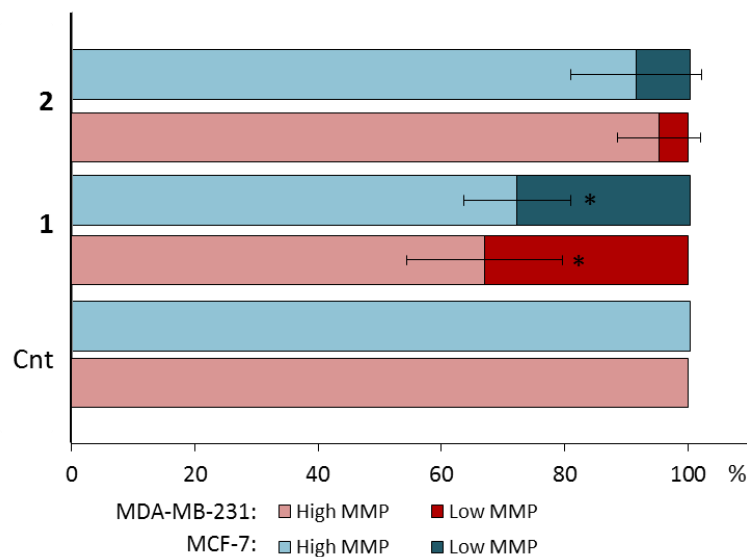


**Figure 7.** Evaluation of MMP in MCF-7 and MDA-MB-231 cells treated with 1 and 2 (40 µM, 18 h) using the probe tetramethylrhodamine methyl ester. The percentage of cells with low and high MMP is shown. \*p<0.05.

### Lipid peroxidation in MDA-MB-231 cells after treatment with 1 or 2

To gain further insight into the mechanism of action of 1 and 2, we tested their ability to induce lipid peroxidation in MDA-MB-231 cells. Lipid peroxidation results from the

attack on (poly)unsaturated lipids by reactive oxygen species (ROS) and is indicative of oxidative stress. The levels of malondialdehyde—the end product of lipid peroxidation—were measured by a fluorimetric assay. The results showed that **1** is able to induce a net 20–30 % increase of malondialdehyde in a concentration-dependent fashion, whereas **2** had no effect (Figure 8).

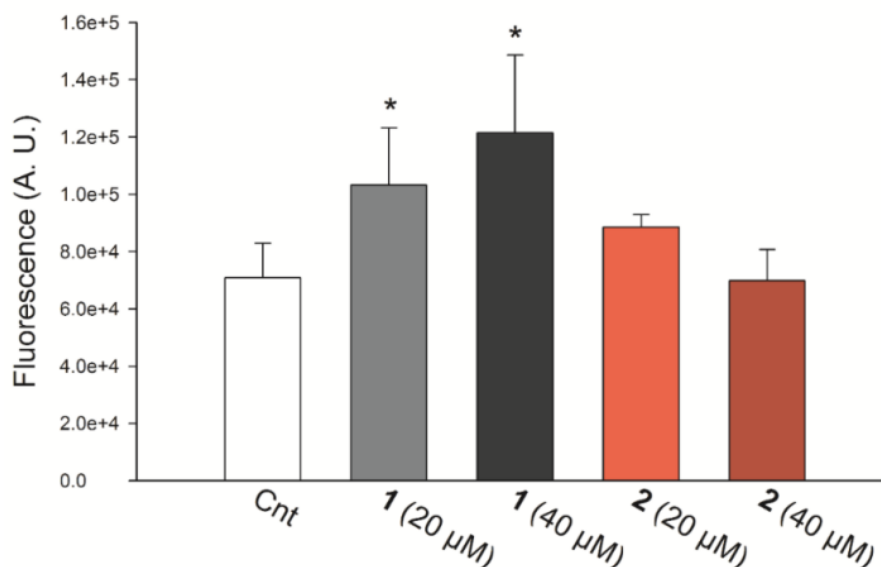


**Figure 8.** Lipid peroxidation induced by **1** and **2** in MDA-MB-231 cells. The amount of coloured adduct was measured with a fluorimetric assay (excitation: 530 nm, emission: 590 nm; see the Experimental Section for details). \* $p < 0.05$ .

## Comparison of the amount of iron in cells incubated with **1** or **2**

Iron was quantified by inductively coupled plasma optical emission spectroscopy (ICP–OES) after incubation of MDA-MB-231 and MCF-7 cell lysates with 40 μM **1** or **2** for 18 h. The results (Table 2) show that the amount of iron found in cells incubated with **1** is significantly higher (2.5-fold) than with **2**. After subtraction of the endogenous iron contribution, the ratio between the amount of **1** and **2** in whole cells was raised to 2.9 in MCF-7 and 6.1 in MDA-MB-231 cells. This difference cannot be explained by different lipophilicity between the two complexes (Log  $P_{o/w}$  = 5.0 for **1**, 4.4 for **2**),<sup>25, 38</sup> but might be related to their difference in cytotoxicity. Indeed, after incubation for 18 h, it is expected that the cytotoxic complex **1** has reacted with specific targets (proteins, DNA, etc.), resulting in its sequestration within cells. By

contrast, the less cytotoxic compound **2** has reacted to a lesser extent, allowing its partial but significant release from the cells.

**Table 2.** Amount of iron [ng per mg protein]<sup>[a]</sup> in MCF-7 and MDA-MB-231 cells incubated with **1** or **2** (40  $\mu$ M) for 18 h, quantified by ICP–OES.

	MCF-7	MDA-MB-231
Control cells	120 $\pm$ 36	110 $\pm$ 50
<b>1</b>	1070 $\pm$ 245	691 $\pm$ 90
<b>2</b>	527 $\pm$ 150	298 $\pm$ 42

<sup>[a]</sup> mean of two experiments  $\pm$  SD

### Quantification of iron in individual cell compartments

MDA-MB-231 and MCF-7 cells were incubated with 40  $\mu$ M **1** for 18 h. Cells were collected and fractionated into crude nuclear, mitochondrial and cytosolic fractions. Iron was quantified in each of these compartments by ICP–OES (Table 3 and Figure S7).

**Table 3.** Subcellular distribution of iron in MCF-7 or MDA-MB-231 cells incubated with 40  $\mu$ M of **1** for 18 h, measured by ICP–OES.

	Cytosolic fraction (%)	Mitochondrial fraction (%)	Crude nuclear fraction (%)
MCF-7 <sup>[a]</sup>	14	35	51
MDA-MB-231 <sup>[b]</sup>	10.8 $\pm$ 0.4	25 $\pm$ 1.6	64.2 $\pm$ 1.3

<sup>[a]</sup>one experiment ; <sup>[b]</sup>mean of 2 experiments

The majority of the iron is located in the crude nuclear fraction. It is slightly higher for MDA-MB-231 cells than for MCF-7 (64.2 % vs. 51 %). The amount of endogenous iron in this fraction is negligible ( $\approx$ 8–10 %). The second largest concentration of iron was found in mitochondria, where it was slightly higher for MCF-7 than for MDA-MB-231 (35 % vs. 25 %). Once again, the contribution of endogenous iron was negligible ( $\approx$ 10 %). Finally, the amount of iron found in cytosol was low in both cell lines, with the proportion of endogenous iron ranging from 25–42 %, depending on the cell line (Figure S7).

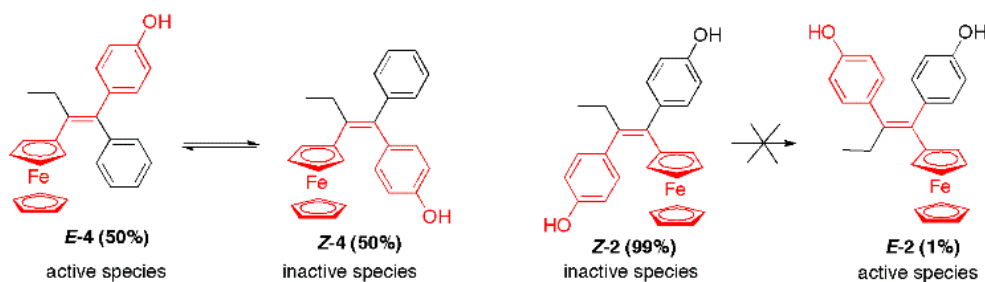
## Discussion

The results obtained with **1** and **2**, not only allow a better understanding of their mechanisms of action, but also explain the difference in their cytotoxicity.

The unique feature common to complexes **1** and **2** is their powerful inhibition of TrxR *in vitro* after enzymatic oxidation by the HRP/H<sub>2</sub>O<sub>2</sub> system (IC<sub>50</sub>≈30 nM). Furthermore, they both interact with its cysteine and selenocysteine residues. This activity is consistent with the fact that in both cases, enzymatic oxidation leads to the formation of a QM that can undergo a 1,8-Michael addition with the cysteine and selenocysteine residues of TrxR. In MDA-MB-231 cells, complex **1** induces only weak inhibition of TrxR and no inhibition in Jurkat cells. This result suggests that inhibition of TrxR is not a critical factor in the cytotoxicity of **1**.

In terms of differences, we note that enzymatic oxidation of **1** by the HRP/H<sub>2</sub>O<sub>2</sub> system involves the ferrocenyl moiety and therefore contrasts with that of its organic analogue **6**; moreover, oxidation of **2** does not proceed by initial reaction at the iron centre but instead mirrors that of the organic compound **7**. This difference appears to be crucial, as the oxidation of FeII to FeIII, which constitutes the first step of the activation of **1** (and **3**) and is accompanied by the production of ROS in variable amounts,<sup>39, 40</sup> is not observed with **2**.<sup>17</sup> It is confirmed here by the effect of **1** on lipid peroxidation, which was not observed with **2**. This process might be associated with the production of ROS, which seemingly play an important role in the cytotoxicity of **1**. Indeed, on MCF-7 cells, co-incubation of **1** with *N*-acetylcysteine, a known antioxidant ROS scavenger, resulted in the loss of its cytotoxic activity (Figure S8).

We have previously demonstrated that the cytotoxicity of ferrocifens is associated with their unique redox properties and the presence of a ferrocenyl–double bond–phenol motif.<sup>14, 17</sup> In the monophenolic complex **4**, or the diphenolic complex **2**, the ferrocenyl and phenol substituents can in principle adopt either *trans* [(*E*)-**4**, (*E*)-**2**] or *cis* [(*Z*)-**4**, (*Z*)-**2**] configurations (Scheme 5). However, as noted above, **2** is found only as the *Z* isomer.



**Scheme 5.** Consequences of the *E/Z* isomerisation of **4** and of the failure of **2** to undergo *E/Z* isomerisation.

It therefore seems plausible to hypothesise that only the *trans* form of the complexes, which exists for **4** and **1**, but not for **2**, facilitates the oxidation of FeII to FeIII, with consequent production of ROS in the cell. This hypothesis also explains the twofold difference in cytotoxicity between **1** and **4** (0.6 and 1.13  $\mu\text{M}$ ).<sup>34</sup>

Because of the approximately equal distribution of the *cis* and *trans* forms of the monophenol **4**, only 50% of the active *E* form is initially present in solution. Of course, in the case of the diphenol **1**, every molecule possesses a phenol substituent *trans* to the ferrocenyl moiety. This assumption is in accordance with the observation that all QMs obtained by the chemical oxidation of ferrocifens that are sufficiently stable to have been characterised unequivocally are exclusively the *E* isomers. This was initially confirmed by the X-ray crystal structure of a QM stabilised by the incorporation of two methyl substituents *ortho* to the carbonyl group,<sup>13</sup> and by another very recent study in which several QMs stabilised by an atypical lone pair– $\pi$  interaction were also structurally characterised.<sup>41</sup>

This result can be explained as follows: let us consider the mechanism of the stepwise oxidation process to form the QM (Scheme S1). To allow delocalisation of the initially formed radical cation from the ferrocenyl to the hydroxy substituent on the phenol, and subsequently from the QM back to the carbon atom adjacent to the ferrocenyl, the connecting framework must be almost planar to favour orbital overlap through the  $\pi$  system. This is ideal in the *E* isomer but would be impossible in the *Z* form, because co-planarity of the  $\text{C}_5\text{H}_5$  ring of the ferrocenyl unit and the *cis*-configured QM ring would engender serious steric problems.

In summary, the lower cytotoxicity of **2** can be explained by the fact that the *Z* configuration of complex **2** does not allow expression of the singular redox effects of ferrocene, which are observed only if the sequence is *trans*-[ferrocene–double bond–phenol]. Molecule **2** can indeed undergo oxidation, but its initial behaviour parallels that of its organic counterpart by forming diquinone **9**, rather than exhibiting the redox effect of ferrocene, which is the origin of the cytotoxicity of **1**.

The results obtained also make it possible to compare the mechanism of action of **1** with that of the tamoxifen-like complex **3** (Figure 1); in particular, they highlight two essential differences. Firstly, **1** barely inhibits thioredoxin reductase activity in Jurkat cells (Figure S6), whereas **3** inhibits it significantly (100 % of inhibition with 15  $\mu$ M **3**).<sup>28</sup> This behaviour is attributed to the cyclisation, in cells, of the QM **8** to form the corresponding indene **14** (Scheme 4).<sup>26</sup> Secondly, **1** does not induce MMP variation in Jurkat cells. This indicates the non-involvement of mitochondria in the cytotoxicity of **1**, in contrast to **3**,<sup>28</sup> thus confirming the essential role played, in this interaction, by the dimethylaminopropyl chain, which confers on **3** the character of a lipophilic cation.<sup>28</sup> Given this observation, the quantities of iron in different cellular compartments (mitochondria, crude nuclear extract, cytosol) might be a surprising result. In fact, a significant percentage of the iron is found in the mitochondria of cells incubated with **1** (35 % in MCF-7 cells, 25 % in MDA-MB-231 cells, Table 3), although the product does not have an effect at 40  $\mu$ M concentration. This confirms the fact, previously observed, that the intracellular sites where complexes are highly concentrated are not necessarily those where they exert their action, but the effects are instead related to their lipophilicity.<sup>42, 43</sup> The quantities of iron found are also similar to those obtained for **4** in Jurkat cells (37 % in the mitochondria of Jurkat cells),<sup>31</sup> a complex whose lipophilicity is close to that of **1** ( $\text{Log } P_{o/w} \approx 4.5$ ).

## Conclusion

Comparisons of the reactivity and the biological behaviour of diphenols **1** and **2** make it possible to better understand their mechanisms of action by highlighting the importance of the *trans* configuration in the ferrocenyl–double bond–phenol sequence for mediating the cytotoxicity of ferrocifens. It also confirms that, although **1** and **3** have similar cytotoxicities on MDA-MB-231 cells, their mechanism of action

differs in some respects. Indeed, in addition to the limited inhibition of TrxR in the cells, we report here that **1** has only a slight effect on mitochondria. This leads to the idea that its mechanism of action is essentially associated with a redox imbalance, as demonstrated by lipid peroxidation and thiol oxidation studies, whereas that of **3** implies an additional effect on mitochondria. Eventually, comparison of the biological behaviour of the highly cytotoxic complex **1**, with that of the poorly cytotoxic complex **2**, let us move forward with respect to understanding the mechanism of action of **1**, one hit in the ferrocifen series.

## Experimental Section

### Materials

Compounds **1** and **2** were synthesised according to literature procedures.<sup>19, 25</sup> Stock solutions (10 mM) were prepared in DMSO.

### Enzymatic oxidation with the mixture HRP/H<sub>2</sub>O<sub>2</sub>

Enzymatic oxidation of the compounds (25–50 μM) by HRP (46 nM) and H<sub>2</sub>O<sub>2</sub> (200 μM) was performed at pH 8.1 in buffer (0.2 M Tris·HCl, 1 mM EDTA) containing 10 % DMSO. HRP (40 μL of 1.14 μM solution) and H<sub>2</sub>O<sub>2</sub> (20 μL of 10 mM solution) were pre-incubated for 5 min and then added to the solution of the compound (940 μL). The solution was immediately transferred to a cuvette and the UV/Vis spectrum was recorded between 250 and 650 or 750 nm on a Cary 50 spectrometer (Varian, Palo Alto, CA). Rate constant  $k_{\text{obs}}$  of oxidation of **1** was calculated by fitting OD<sub>560nm</sub> versus time data according to the first-order law Equation 1 with KaleidaGraph software ( $C_0$  corresponds to the absorbance at infinite time, while  $C_1$  is the difference between absorbance at 0 time and absorbance at infinite time).

$$\text{OD} = C_0 + C_1 \times \exp(-k_{\text{obs}} \times t)$$

### TrxR1 activity in vitro

Thioredoxin reductase activity was determined by measuring the ability of TrxR1 to reduce 5,5'-dithiobis(2-nitrobenzoic acid) (DTNB) in the presence of NADPH. Aliquots of highly purified TrxR1 in Tris·HCl buffer (0.2 M, pH 8.1) containing EDTA (1 mM) and NADPH (0.25 mM) were preincubated for 5 min with the compounds. Then, the reaction was initiated with DTNB (1 mM) and monitored spectrophotometrically at 412 nm for approximately 10 min. For the oxidation of **1** and **2** in order to obtain ferrociphenol derivatives, freshly prepared compounds, at increasing concentrations, were incubated for 15 min in Tris·HCl buffer (0.2 M, pH 8.1) containing EDTA (1 mM), H<sub>2</sub>O<sub>2</sub> (0.1 mM) and HRP (22 nM). Then, TrxR1 and NADPH (0.25 mM) were added and mixtures were incubated for another 5 min. Finally, the reaction was initiated with DTNB (1 mM) and monitored spectrophotometrically at 412 nm for approximately 10 min.

### **BIAM assay**

Compounds **1** and **2** (4 μM) were treated with a mixture of HRP (22 nM) and H<sub>2</sub>O<sub>2</sub> (0.1 mM) for 15 min. Then, TrxR1 (1 μM) pre-reduced with NADPH (60 μM), was incubated for 30 min with the compounds or their derivatives (2 μM) in Tris·HCl buffer (50 mM, pH 7.4) containing NADPH (200 μM) and EDTA (1 mM). After incubation, a sample of the reaction mixture (8 μL) was added to BIAM (100 mM, 8 μL) in Tris·HCl (0.1 M, pH 8.5) or HEPES-Tris (0.1 M, pH 6.0) buffers. Samples were incubated at RT for an additional 30 min to allow BIAM alkylation of free SH/SeH groups of the enzyme. Then, BIAM-modified enzyme was subjected to SDS-PAGE (10 % gel) and transferred to a nitrocellulose membrane. BIAM-labelled enzyme was detected using HRP-conjugated streptavidin and enhanced chemiluminescence detection.

### **MTT proliferation assay**

Cells (5×10<sup>3</sup>) were seeded in a 96-well plate and treated with the compounds dissolved in DMSO. After 72 h, the medium was removed and MTT solution (0.5 mg mL<sup>-1</sup>, 100 μL) in PBS (1×) was added. After 3 h in the dark at 37° C and 5 % CO<sub>2</sub>, the MTT solution was gently aspirated and the reaction was quenched with

isopropanol/DMSO (9:1, 100  $\mu$ L). Then, the absorbance was recorded (A595–690) using a plate reader (Tecan Infinite M200 PRO, Männedorf, Switzerland).

### **TrxR and GR activities in cell lysates**

Cells ( $1 \times 10^6$ ) were incubated for 18 h in the presence of the compounds and then harvested and washed with PBS. Each sample was lysed with a modified radioimmunoprecipitation assay (RIPA) buffer: NaCl (150 mM), Tris·HCl (50 mM), EDTA (1 mM), 1 % Triton X-100, 0.1 % SDS, 0.5 % sodium deoxycholate, NaF (1 mM) and an antiprotease cocktail (Complete, Roche, Mannheim, Germany) containing phenylmethylsulfonyl fluoride (PMSF, 0.1 mM). After 40 min at 4 °C, the lysates were centrifuged at 12 000 g, to discard the debris, and tested for total TrxR activity. The reaction was started by the addition of DTNB (0.1 M). The absorbance of the DTNB reduction product was monitored at 412 nm at 25 °C. GR activity of cell lysates was measured in Tris·HCl buffer (0.2 M, pH 8.1) containing EDTA (1 mM) and NADPH (0.25 mM). The assay was initiated by addition of glutathione disulfide (1 mM) and monitored spectrophotometrically at 340 nm.

### **Total thiol assay**

MDA-MB-231 and MCF-7 cells ( $3.5 \times 10^5$ ) were seeded in six-well plates and treated with the compounds. After 18 h, the plates were washed with PBS (1 $\times$ , 1 mL). Cells were then dissolved with Tris·HCl (0.2 M, pH 8.1, 1 mL), EDTA (5 mM) and guanidine (7.2 M). The reaction was started by the addition of DTNB (0.1 M). The absorbance of the product of DTNB reduction was monitored at 412 nm at 25 °C.

### **Mitochondrial membrane potential assay**

Cells ( $1 \times 10^6$ ) were seeded in 25 cm<sup>2</sup> flasks and then treated with the compounds for 18 h. Subsequently, the cells were washed with PBS (1 $\times$ ) and glucose (10 mM), trypsinised and centrifuged at 500 g for 5 min. Then, cells ( $2.5 \times 10^5$  per tube) were resuspended in PBS (1 $\times$ ) and glucose (10 mM) and incubated with the fluorescent probe TMRM (25 nM, Thermo Fisher Scientific, Waltham, MA) for 20 min. FACS

analysis of TMRM was performed on a FACSCanto II flow cytometer (Becton Dickinson, Franklin Lakes, NJ).

### **Lipid peroxidation assay**

Cells ( $1 \times 10^6$ ) were treated with compounds at different concentrations for 18 h. Next, cells were washed with PBS and disrupted with  $\text{H}_2\text{SO}_4$  (50 mM, 1 mL) and 10 % phosphotungstic acid (150  $\mu\text{L}$ ) for 10 min at RT. Then, cells were scraped and centrifuged at 15 600 g for 10 min at 4° C. The obtained pellets were washed with  $\text{H}_2\text{SO}_4$  (50 mM, 1 mL) and 10 % phosphotungstic acid (150  $\mu\text{L}$ ). Samples were kept at RT for 5 min and centrifuged at 15 600 g for 10 min at 4 °C. Next, the pellets were dissolved with 0.25 % Nonidet P-40 (350  $\mu\text{L}$ ) containing 0.01 % butylhydroxytoluene and 0.17 % thiobarbituric acid, and incubated at 95° C for 60 min. Samples, were cooled on ice for 5 min and centrifuged at 15 600 g for 10 min. The supernatants were added to *n*-butanol (400  $\mu\text{L}$ ), vigorously mixed and centrifuged at 15 600 g for 15 min. The fluorescence of the upper phase was analysed (Ex=530 nm, Em=590 nm) using a plate reader (Tecan Infinite M200 PRO, Männedorf, Switzerland). The discarded pellets were solubilised and subjected to protein determination.

### **Preparation of cellular sub-fractions**

Cells were sub-fractionated by essentially following a published protocol.<sup>28</sup> In brief, cells ( $3 \times 10^7$ ) were collected, washed with PBS and subjected to hypo-osmotic treatment with Tris·HCl buffer (10 mM, pH 7.5, 2 mL) containing NaCl (10 mM) and  $\text{MgCl}_2$  (1.5 mM) for 5 min and gently homogenised using a Dounce tissue grinder. Then, Tris·HCl buffer (12.5 mM, pH 7.5, 1.4 mL) containing mannitol (525 mM), sucrose (175 mM) and EDTA (2.5 mM) was rapidly added. The homogenate was diluted to a final volume of 5 mL with mannitol (210 mM), sucrose (70 mM), EDTA (1 mM), Tris·HCl buffer (5 mM, pH 7.5) and subjected to differential centrifugation. The first step was carried out at 1300 g for 5 min at 4° C to discard nuclei and non-disrupted cells. The mitochondrial fraction was isolated from the supernatant at 15 800 g for 15 min at 4° C and washed twice. The crude soluble supernatant obtained from the mitochondria isolation step was further centrifuged at 105 000 g for

15 min at 4 °C to obtain the cytosolic fraction. Mitochondrial fractions were lysed using a modified RIPA buffer containing Tris·HCl (50 mM, pH 7.4), NaCl (150 mM), EDTA (1 mM), 1 % Triton X100, 0.1 % SDS, 0.5 % DOC and NaF (1 mM), supplemented with an antiprotease cocktail and PMSF (0.1 mM), and subjected to protein determination using the Lowry assay.<sup>44</sup> The presence of cytochrome oxidase and cytochrome c as mitochondrial markers was assessed by western blot analysis of the mitochondrial fraction.

### **Iron assay by ICP–OES**

Cells incubated for 18 h in the presence of the compounds (40 µM) were collected as cell lysates (starting from  $1 \times 10^6$  cells) or subjected to cell fractionation (starting from  $24 \times 10^6$  cells) as described in a previous section. Cell lysates, mitochondria and crude nuclei fractions were dissolved in concentrated nitric acid (70 %, ACS grade, 0.286 mL) and digested at 60 °C in an ultrasonic bath for 1 h. Then the sample volume was adjusted to 10 mL by addition of water (final concentration of HNO<sub>3</sub> in the sample was 2 %). The cytosol samples were adjusted to 2 % HNO<sub>3</sub> by addition of proper volumes of HNO<sub>3</sub> and water (final volume of 10 mL Milli-Q grade water) and kept at 4 °C for 48 h. Samples were clarified by brief centrifugation at 2600 g for 5 min and filtered on a 0.22 µm PES membrane. Quantification of iron was performed at 238.204 nm using an Agilent 5100 instrument (Santa Clara, CA). Iron standards were prepared from a 1000 ppm stock solution (Iron standards for ICP, Fluka). The concentrations used for calibration were 0, 7.8, 15.6, 31.2, 62.5, 125, 250 and 500 ppb. Measurements were performed in triplicate in two or three sets of independent experiments. ICP–OES experiments were performed on an Agilent 5100 SVDV at the ALIPP6 laboratory (ISTeP, Sorbonne Université).

### **Acknowledgements**

M.P.R. and V.S. acknowledge BIRD187299/18 granted by the University of Padova (Italy). We thank Sébastien Blanchard (IPCM, Sorbonne Université) for the EPR measurements.

## Conflict of interest

The authors declare no conflict of interest.

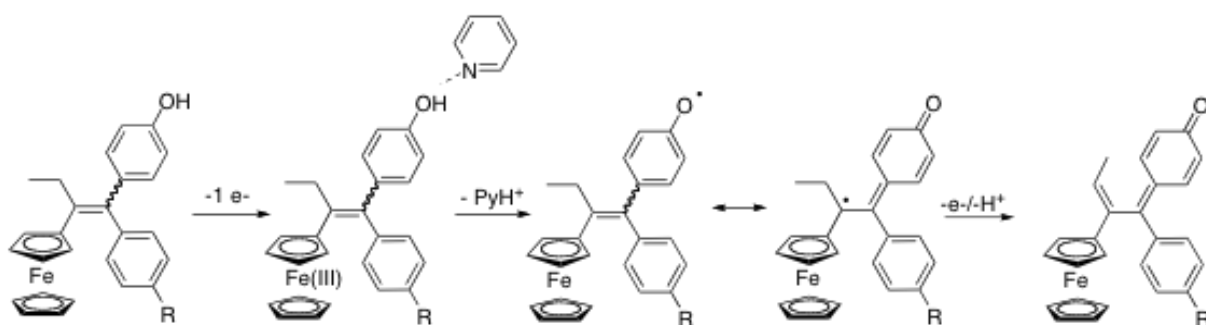
## References

- 1 N. P. E. Barry, P. J. Sadler, *Chem. Commun.* **2013**, 49, 5106–5131.
- 2 G. Gasser, I. Ott, N. Metzler-Nolte, *J. Med. Chem.* **2011**, 54, 3–25.
- 3 E. Wong, C. M. Giandomenico, *Chem. Rev.* **1999**, 99, 2451–2466.
- 4 C. G. Hartinger, P. J. Dyson, *Chem. Soc. Rev.* **2009**, 38, 391–401.
- 5 P. Y. Zhang, P. J. Sadler, *J. Organomet. Chem.* **2017**, 839, 5–14.
- 6 B. Albada, N. Metzler-Nolte, *Chem. Rev.* **2016**, 116, 11797–11839.
- 7 S. M. Meier-Menches, C. Gerner, W. Berger, C. G. Hartinger, B. K. Keppler, *Chem. Soc. Rev.* **2018**, 47, 909–928.
- 8 E. A. Hillard, A. Vessières, G. Jaouen in *Medicinal Organometallic Chemistry*, Springer-Verlag, Berlin, **2010**, pp. 81–117.
- 9 G. Jaouen, S. Top in *Advances in Organometallic Chemistry and Catalysis*, Wiley, Hoboken, **2014**, pp. 561–580.
- 10 G. Jaouen, A. Vessières, S. Top, *Chem. Soc. Rev.* **2015**, 44, 8802–8817.
- 11 A. Vessières, *J. Organomet. Chem.* **2013**, 734, 3–16.
- 12 A. Vessieres in *Metal-Based Anticancer Agents*, Royal Society of Chemistry, Cambridge, **2019**, pp. 62–90.
- 13 D. Hamels, P. M. Dansette, E. A. Hillard, S. Top, A. Vessières, P. Herson, G. Jaouen, D. Mansuy, *Angew. Chem. Int. Ed.* **2009**, 48, 9124–9126.
- 14 P. Messina, E. Labbé, O. Buriez, E. A. Hillard, A. Vessières, D. Hamels, S. Top, G. Jaouen, Y. M. Frapart, D. Mansuy, C. Amatore, *Chem. Eur. J.* **2012**, 18, 6581–6587.
- 15 Y. Wang, M. A. Richard, S. Top, P. M. Dansette, P. Pigeon, A. Vessières, D. Mansuy, G. Jaouen, *Angew. Chem. Int. Ed.* **2016**, 55, 10431–10434.
- 16 Y. Wang, P. M. Dansette, P. Pigeon, S. Top, M. J. McGlinchey, D. Mansuy, G. Jaouen, *Chem. Sci.* **2018**, 9, 70–78.
- 17 E. A. Hillard, A. Vessières, L. Thouin, G. Jaouen, C. Amatore, *Angew. Chem. Int. Ed.* **2006**, 45, 285–290.

- 18 G. Jaouen, S. Top, A. Vessières, G. Leclercq, J. Quivy, L. Jin, A. Croisy, C. R. Acad. Sci., Ser. Ilc: Chim. **2000**, 3, 89–93.
- 19 S. Top, A. Vessières, G. Leclercq, J. Quivy, J. Tang, J. Vaissermann, M. Huché, G. Jaouen, *Chem. Eur. J.* **2003**, 9, 5223–5236.
- 20 M. Görmen, P. Pigeon, S. Top, E. A. Hillard, M. Huché, C. G. Hartinger, F. de Montigny, M.-A. Plamont, A. Vessières, G. Jaouen, *ChemMedChem* **2010**, 5, 2039–2050.
- 21 E. Allard, C. Passirani, E. Garcion, P. Pigeon, A. Vessières, G. Jaouen, J. P. Benoit, *J. Controlled Release* **2008**, 130, 146–153.
- 22 C. Bruyère, V. Mathieu, A. Vessières, P. Pigeon, S. Top, G. Jaouen, R. Kiss, *J. Inorg. Biochem.* **2014**, 141, 144–151.
- 23 Q. Michard, G. Jaouen, A. Vessières, B. A. Bernard, *J. Inorg. Biochem.* **2008**, 102, 1980–1985.
- 24 Y. L. K. Tan, P. Pigeon, E. A. Hillard, S. Top, M.-A. Plamont, A. Vessières, M. J. McGlinchey, H. Mueller-Bunz, G. Jaouen, *Dalton Trans.* **2009**, 10871–10881.
- 25 A. Vessières, S. Top, P. Pigeon, E. A. Hillard, L. Boubeker, D. Spera, G. Jaouen, *J. Med. Chem.* **2005**, 48, 3937–3940.
- 26 A. Citta, A. Folda, A. Bindoli, P. Pigeon, S. Top, A. Vessières, M. Salmain, G. Jaouen, M. P. Rigobello, *J. Med. Chem.* **2014**, 57, 8849–8859.
- 27 V. Scalcon, A. Bindoli, M. P. Rigobello, *Free Radical Biol. Med.* **2018**, 127, 62–79.
- 28 V. Scalcon, M. Salmain, A. Folda, S. Top, P. Pigeon, H. Z. S. Lee, G. Jaouen, A. Bindoli, A. Vessières, M. P. Rigobello, *Metallomics* **2017**, 9, 949–959.
- 29 Ö. Karaca, V. Scalcon, S. M. Meier-Menches, R. Bonsignore, J. M. J. L. Brouwer, F. Tonolo, A. Folda, M. P. Rigobello, F. E. Kühn, A. Casini, *Inorg. Chem.* **2017**, 56, 14237–14250.
- 30 E. Schuh, C. Pflüger, A. Citta, A. Folda, M. P. Rigobello, A. Bindoli, A. Casini, F. Mohr, *J. Med. Chem.* **2012**, 55, 5518–5528.
- 31 V. W. Winkler, M. A. Nyman, R. S. Egan, *Steroids* **1971**, 17, 197.
- 32 Y. Ortin, J. Grealis, C. Scully, H. Muller-Bunz, A. R. Manning, M. J. McGlinchey, *J. Organomet. Chem.* **2004**, 689, 4683–4690.
- 33 V. Scalcon, A. Citta, A. Folda, A. Bindoli, M. Salmain, I. Ciofini, S. Blanchard, J. D. Cazares-Marinero, Y. Wang, P. Pigeon, G. Jaouen, A. Vessières, M. P. Rigobello, *J. Inorg. Biochem.* **2016**, 165, 146–151.

- 34 H. Z. S. Lee, O. Buriez, F. Chau, E. Labbé, R. Ganguly, C. Amatore, G. Jaouen, A. Vessières, W. K. Leong, S. Top, *Eur. Inorg. Chem.* **2015**, 4217–4225.
- 35 G. H. Degen, J. A. McLachlan, *Chem.-Biol. Interact.* **1985**, 54, 363–375.
- 36 V. Scalcon, S. Top, H. Z. S. Lee, A. Citta, A. Folda, A. Bindoli, W. K. Leong, M. Salmain, A. Vessières, G. Jaouen, M. P. Rigobello, *J. Inorg. Biochem.* **2016**, 160, 296–304.
- 37 M.-A. Richard, D. Hamels, P. Pigeon, S. Top, P. M. Dansette, H. Z. S. Lee, A. Vessières, D. Mansuy, G. Jaouen, *ChemMedChem* **2015**, 10, 981–990.
- 38 E. A. Hillard, A. Vessières, S. Top, P. Pigeon, K. Kowalski, M. Huché, G. Jaouen, *J. Organomet. Chem.* **2007**, 692, 1315–1326.
- 39 C. Lu, J. M. Heldt, M. Guille-Collignon, F. Lemaitre, G. Jaouen, A. Vessières, C. Amatore, *ChemMedChem* **2014**, 9, 1286–1293.
- 40 A. Vessières, C. Corbet, J. M. Heldt, N. Lories, N. Jouy, I. Laios, G. Leclercq, G. Jaouen, R. A. Toillon, *J. Inorg. Biochem.* **2010**, 104, 503–511.
- 41 Y. Wang, P. Pigeon, S. Top, J. Sanz Garcia, C. Troufflard, I. Ciofini, M. J. McGlinchey, G. Jaouen, *Angew. Chem. Int. Ed.* **2019**, 58, 8421–8425.
- 42 S. Clède, F. Lambert, C. Sandt, S. Kascakova, M. Unger, E. Harte, M. A. Plamont, R. Saint-Fort, A. Deniset-Besseau, Z. Gueroui, C. Hirschmugl, S. Lecomte, A. Dazzi, A. Vessières, C. Policar, *Analyst* **2013**, 138, 5627–5638.
- 43 F. Fus, Y. Yang, H. Z. S. Lee, S. Top, M. Carriere, A. Bouron, A. Pacureanu, J. C. da Silva, M. Salmain, A. Vessières, P. Cloetens, G. Jaouen, S. Bohic, *Angew. Chem. Int. Ed.* **2019**, 58, 3461–3465.
- 44 O. H. Lowry, N. J. Rosebrough, A. L. Farr, R. J. Randall, *J. Biol. Chem.* 1951, 193, 265–275.

## SUPPLEMENTARY MATERIAL



**Scheme S1.** Mechanism of formation of quinone methides.

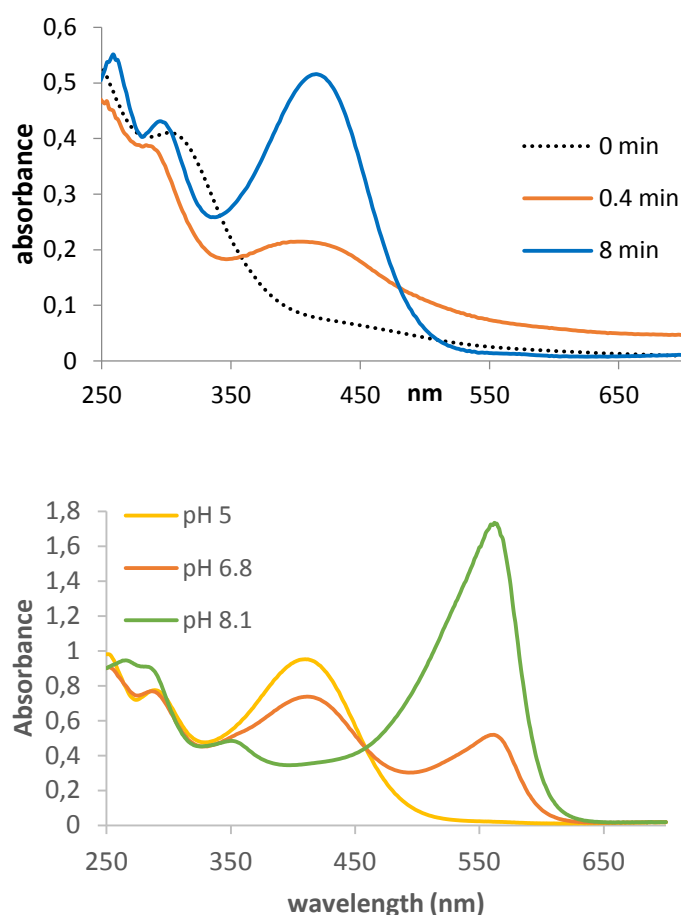


**Figure S1.** Upper panel: Time evolution of the UV-Vis spectrum of **1** (50  $\mu$ M) incubated at 25  $^{\circ}$ C in the presence of HRP (46 nM) and  $H_2O_2$  (200  $\mu$ M) in citrate-phosphate buffer pH 5 (48.5 mM citric acid and 103 mM  $Na_2HPO_4$ ) containing 10% DMSO. Pure **1** (0 min): band at 304 nm; after 0.4 min: bands at 406 nm (broad), 286 nm (shoulder); after 8 min: bands at 416 nm (intense), 296 and 262 nm. Lower panel: uv-visible spectra of mixtures of **1** (50  $\mu$ M), HRP (46 nM) and  $H_2O_2$  (200  $\mu$ M) in buffer containing 10% DMSO at various pH. Spectra measured after 2 min incubation at 25 $^{\circ}$ C.

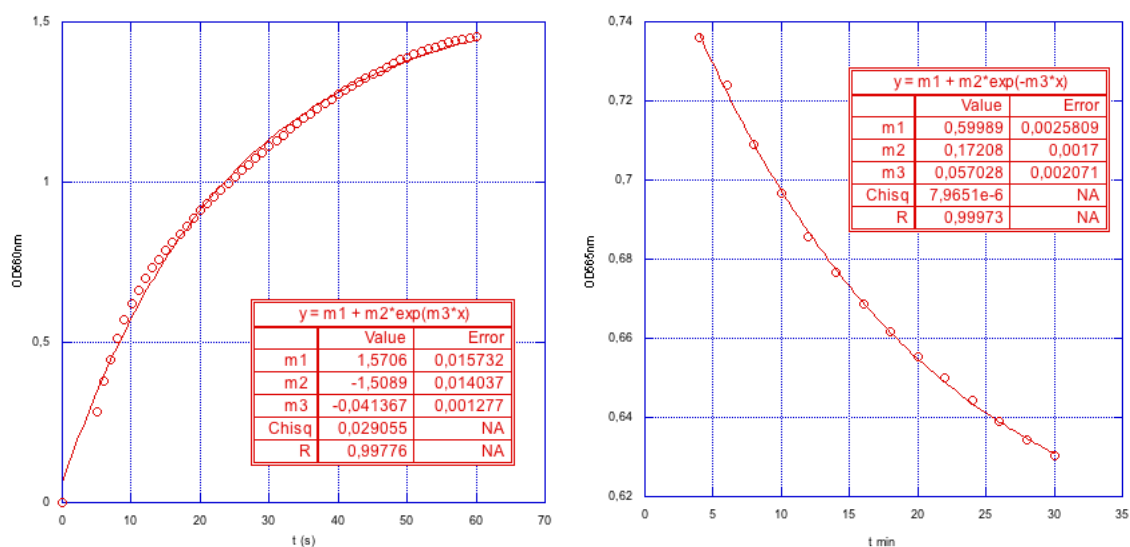


**Figure S2.** Enzymatic oxidation of **1** (50  $\mu\text{M}$ ) by HRP (46 nM) and  $\text{H}_2\text{O}_2$  (200  $\mu\text{M}$ ) in Tris-HCl buffer pH 8.1 containing 10% DMSO. Kinetic study of the formation (left panel) and degradation (right panel) of **8A** measured at 560 nm.

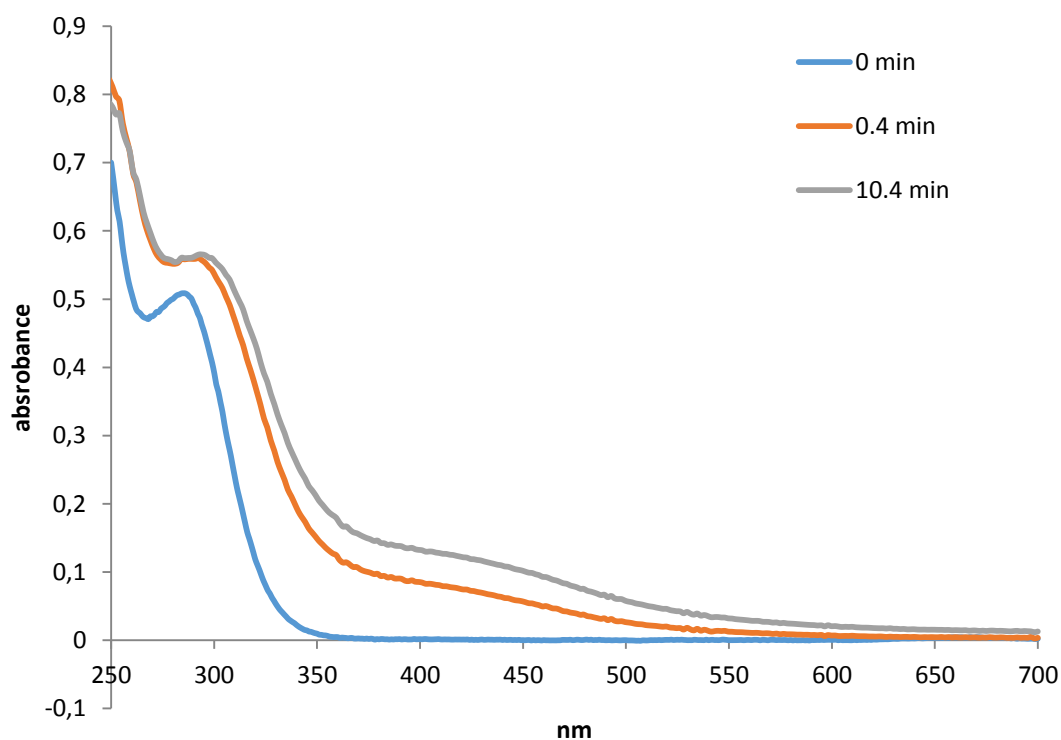


**Figure S3.** Time evolution of the UV-Vis spectrum of **6** (50  $\mu\text{M}$ ) incubated at 25  $^\circ\text{C}$  in the presence of HRP (46 nM) and  $\text{H}_2\text{O}_2$  (200  $\mu\text{M}$ ) in citrate-phosphate buffer pH 5 (48.5 mM citric acid and 103 mM Na phosphate dibasic) containing 10% DMSO. Pure **6** (0 min): band at 285 nm; after 0.4 and 10.4 min: peak at 296 nm.

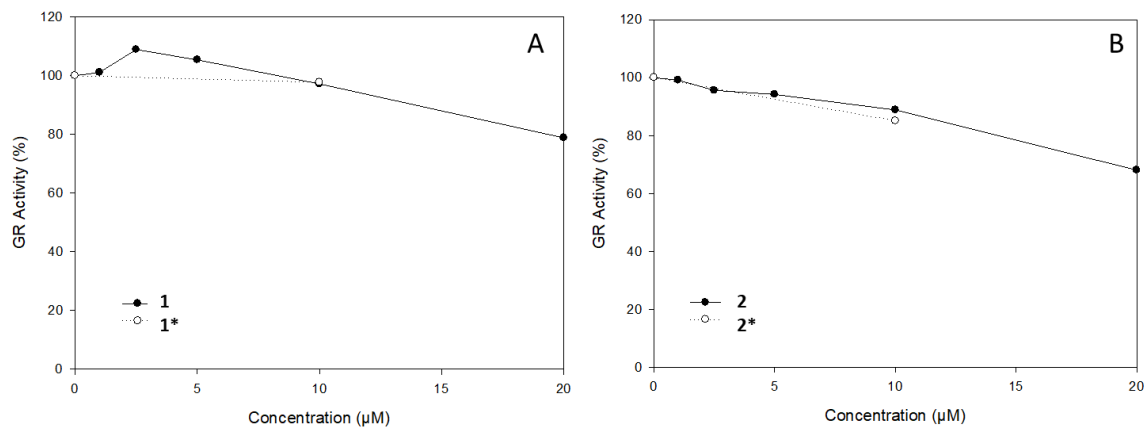


**Figure S4.** *In vitro* inhibition of GR by 1 and 1\* (A), 2 and 2\* (B).

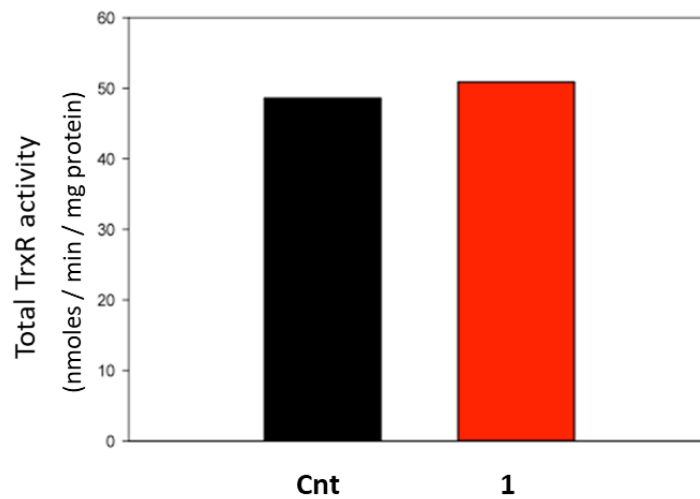


**Figure S5.** Effect of 1 (15 μM) on TrxR activity in Jurkat cells after treatment for 18 h.

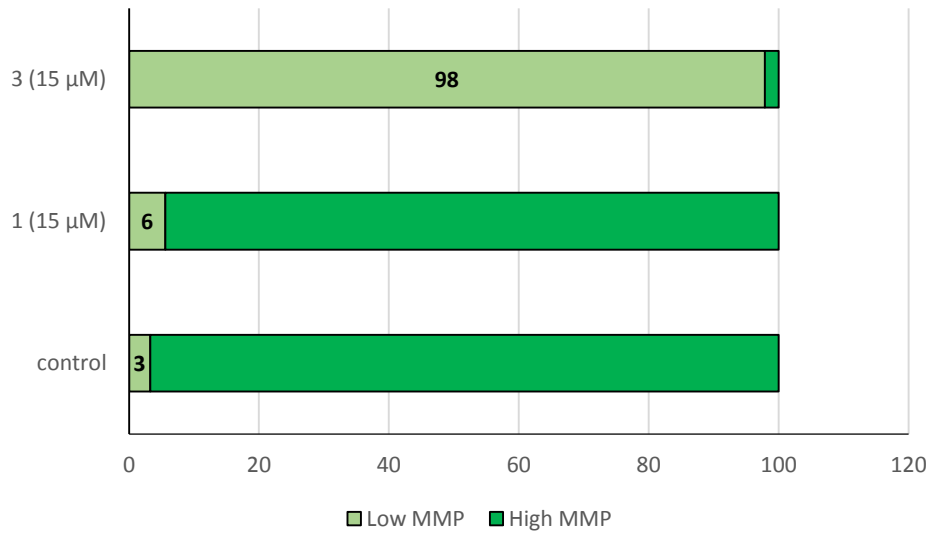


**Figure S6.** Percentage of Jurkat cells with low and high MMP after incubation with **1** or **3** (15 μM, 18 h).

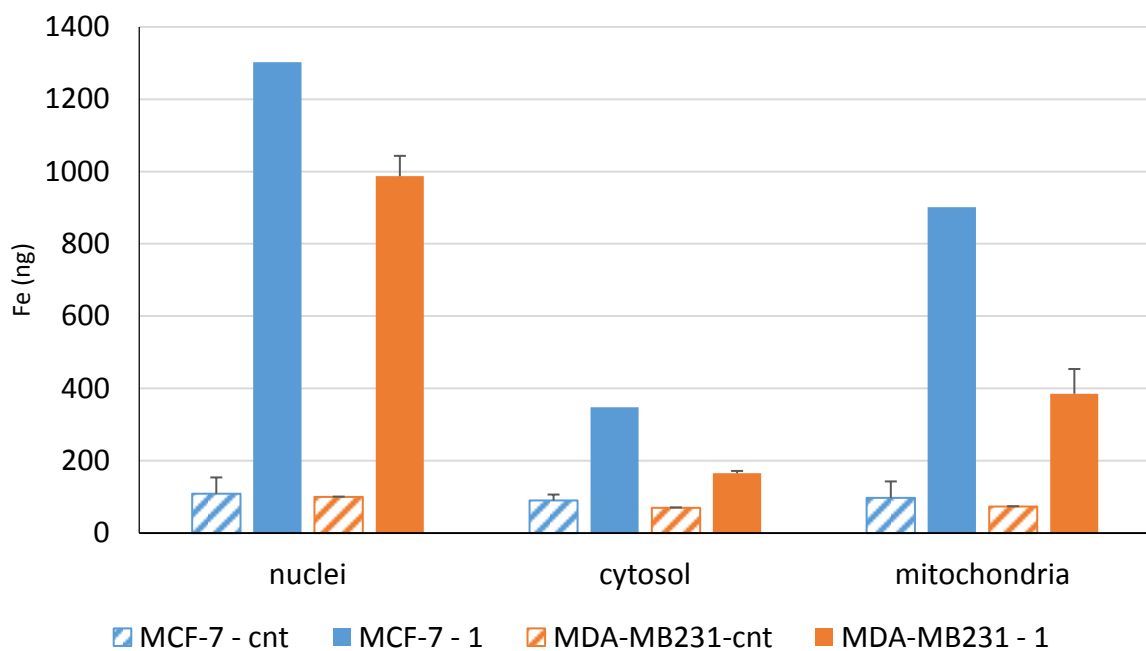


**Figure S7.** Iron quantity (ng) in subcellular fractions measured by ICP-OES. Cells were incubated with 40 μM compound **1** for 18 h and fractionated as described in the Experimental Section.

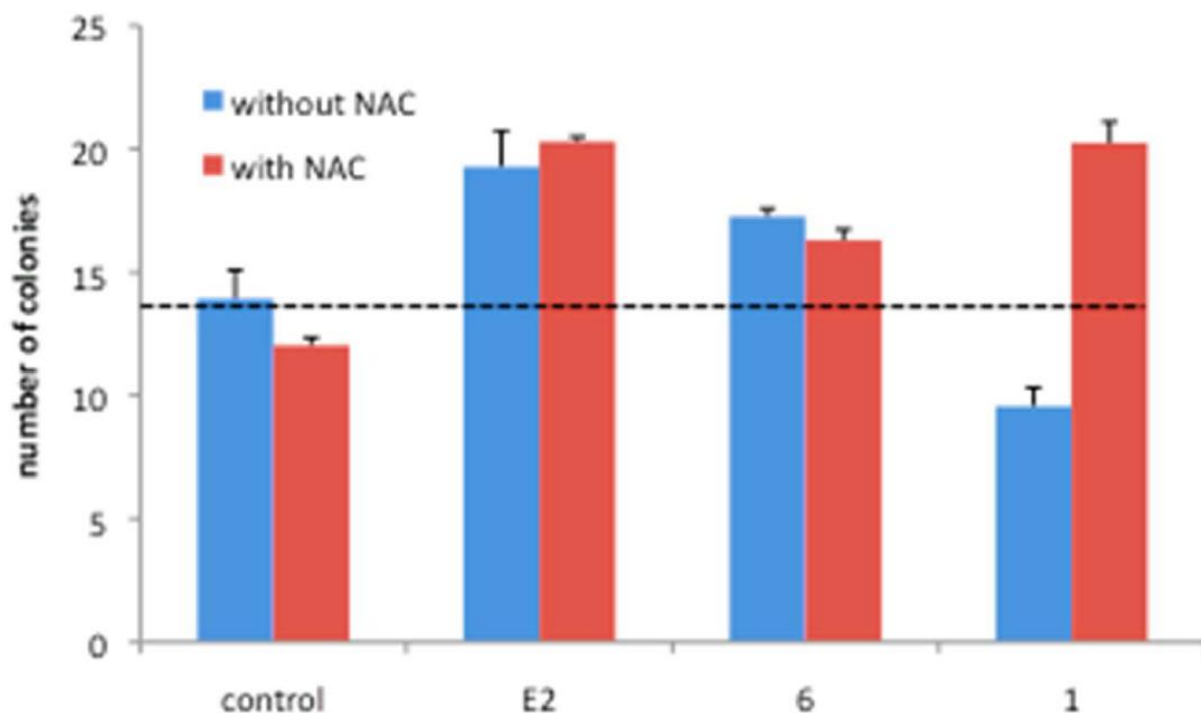


**Figure S8.** Clonogenic assay in soft agar, on MCF-7 cells (hormone dependent breast cancer cells) incubated with **1** and **6** (1  $\mu\text{M}$ ) for 21 days, in the presence or absence of the antioxidant N-acetyl cysteine (NAC, 10 mM). Mean of 3 experiments. Addition of the antioxidant NAC reversed the cytotoxic effect of **1**, demonstrating the role, played by ROS in the expression of its cytotoxicity. It also allows the expression of its estrogenic (proliferative) activity which is almost the same as the one observed with of 1 nM of estradiol (E2). This estrogenic (proliferative effect) is also observed with **6** without or with NAC. Experiment was performed as described by: Vessières et al. *J. Inorg. Biochem.*, 2010, 104, 503-510.